Published in final edited form as:
Acc Chem Res. 2008 December ; 41(12): 1587–1595. doi:10.1021/ar800018v.

Gold Nanocages: Synthesis, Properties, and Applications

SARA E. SKRABALAK[†], **JINGYI CHEN**[†], **YUGANG SUN**[†], **XIANMAO LU**[‡], **LESLIE AU**[†], **LAIRE M. COBLEY**[‡], and **YOUNAN XIA**[†,‡,*]

† *Department of Chemistry, University of Washington, Seattle, Washington 98195*

‡ *Department of Biomedical Engineering, Washington University, Saint Louis, Missouri 63130*

Conspectus

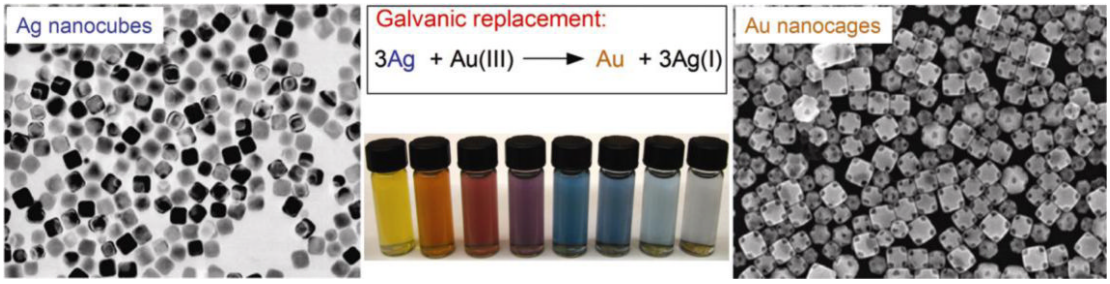

Noble-metal nanocages represent a novel class of nanostructures with hollow interiors and porous walls. They are prepared using the remarkably simple galvanic replacement reaction between solutions containing metal precursor salts and Ag nanostructures prepared by polyol reduction. The electrochemical potential difference between the two species drives the reaction, with the reduced metal depositing on the surface of the Ag nanostructure. In our most studied example involving $HAuCl_4$ as the metal precursor, the resultant Au epitaxially deposits on the surface of the Ag nanocubes, adopting their cubic structure. Concurrent with this deposition, the interior Ag is oxidized and removed, together with alloying and dealloying, to produce hollow and eventually porous structures that we commonly refer to as Au nanocages. This approach has proven versatile, with a wide range of morphologies – including nanorings, prism-shaped nanoboxes, nanotubes, and multiple-walled nanoshells or nanotubes – being produced by changing the shape of the initial Ag template. Besides Au-based structures, Pt- and Pd-containing hollow nanostructures have been prepared by switching the metal salt precursors to Na_2PtCl_4 or Na_2PdCl_4, respectively.

Additionally, we have found it easy to tune both the composition and localized surface plasmon resonance (LSPR) of the metal nanocages by simply changing the amount of metal precursor added to the suspension of Ag nanocubes. In this way, we are developing these structures for biomedical and catalytic applications. As the Au nanocages are predicted by discrete dipole approximations (DDA) to have large absorption cross-sections and their LSPR can be tuned into the near-infrared where the attenuation of light by blood and soft tissue is greatly reduced, they are attractive for biomedical applications in which the selective absorption of light at great depths is desirable. For example, we have explored their use as contrast enhancement agents for both optical coherence tomography (OCT) and photoacoustic tomography (PAT), with improvements being observed in each case. As the Au nanocages have large absorption cross-sections, they are also effective photothermal transducers, which when targeted to cancer cells could provide a therapeutic effect by selectively killing them by hyperthermia. Our *in vitro* work illustrates the feasibility of this technique as a less invasive form of cancer treatment.

*To whom correspondence should be addressed. E-mail: xia@biomed.wustl.edu.

Introduction

Owing to the unique and tunable optical, electronic, and catalytic properties of noble-metal nanostructures, the synthesis and utilization of such structures in various applications have been reported widely.[1-5] The properties of metal nanostructures can be tailored by controlling their composition, size, shape, and structure (hollow *vs.* solid).[6-9] This notion has led to single-component metal nanostructures being synthesized as nanowires,[10] nanorods,[11-13] nanospheres,[14] nanoplates,[15-17] and nanocubes,[18-20] among others.[21-23] To introduce compositional and structural complexity, we use galvanic replacement reactions as a general route to hollow, multi-metal nanostructures.[24] Here, we highlight advances from our laboratory on the synthesis and use of gold-based nanocages – hollow, porous structures with dimensions < 100 nm.

The galvanic replacement reaction represents a simple means of preparing multi-metal hollow structures. The electrochemical potential difference between two metals drives the reaction, with one serving as the cathode and the other as the anode. The classic example is of a zinc strip in a solution containing Cu^{2+} ions. As the Zn^{2+}/Zn reduction potential is more negative than the Cu^{2+}/Cu potential (−0.76 V and 0.34 V *vs.* the standard hydrogen electrode, SHE, respectively), Zn is oxidized to Zn^{2+} while Cu^{2+} is reduced to Cu. Significantly, this phenomenon is extendable to other systems, and as we found, the metal strip can be replaced with metal nanostructures.

Regarding the preparation of Au-based nanocages, the reduction potential of $AuCl_4^-/Au$ (0.99 V *vs.* SHE) is more positive than that of AgCl/Ag (0.22 V *vs.* SHE).[25] Thus, Ag nanocubes[18,26] can serve as a template for reaction, being oxidized by $HAuCl_4$ according to:

$$3Ag_{(s)} + HAuCl_{4(aq)} \rightarrow Au_{(s)} + 3AgCl_{(s)} + HCl_{(aq)} \quad (1)$$

The produced Au is confined to the nanocube surface, growing on it and adopting its morphology as interior Ag is oxidized to produce a hollow structure. In principle, this Ag template-engaged replacement reaction can be applied to any metal whose redox potential is more positive than the AgCl/Ag pair, although morphology differences have been observed in other systems. We begin by describing the mechanism for nanocage formation, followed by a discussion of their properties and potential uses.

Formation of Au-Based Nanocages

The Ag template-engaged galvanic replacement reaction is run like a titration, with $HAuCl_4$ solution (for Au-based nanocages) being controllably added to a boiling suspension of Ag nanocubes. The morphological and compositional changes at various stages of replacement were monitored using scanning electron microscopy (SEM), transmission electron microscopy (TEM), and elemental analysis. The results provide insight into the formation of hollow, porous nanostructures.[27] These results also contrast with those obtained when Ag nanocubes with rounded corners were used.[28]

After Ag nanocubes with sharp corners (Figure 1A) react with a small amount of $HAuCl_4$ solution, a pinhole is observed on one of the six faces of each cube (Figure 1B), indicating that the reaction is initiated locally at a high-energy site (e.g., surface step, point defect, or hole in capping layer)[29] rather than over the entire cube surface. As the reaction proceeds, this pinhole serves as the anode, where Ag is oxidized and electrons are stripped. The released electrons migrate to the nanocube faces and are captured by $AuCl_4^-$, generating Au atoms that epitaxially grow on the nanocube. As the Au layer forms, the initial pinhole serves as the site for Ag

dissolution, facilitating the conversion of the nanocube into a nanobox (Figure 1B, upper inset). In later stages of reaction, the pinhole closes (Figure 1C), presumably through mass diffusion processes and/or direct deposition of Au near the pinhole. TEM of a microtomed sample reveals the hollow interior of the nanobox (Figure 1C, upper inset).

Characterization of these nanostructures by electron diffraction and TEM indicates that they are single-crystalline, composed of a homogeneous Au/Ag alloy and not a heterogeneous, mosaic structure. This observation is unsurprising given the mutual solubility of Ag and Au and the high diffusion rates expected at the reaction temperature.[30,31] In the later stages of reaction, inductively coupled plasma-atomic emission spectroscopy (ICP-AES) indicates that the atomic ratio of Au and Ag in the structures deviates from the relationship described by Equation 1, with more $HAuCl_4$ solution being necessary to oxidize the Ag nanocubes. We attribute this discrepancy to the higher potential required to oxidize Ag atoms comprised in a Ag/Au alloy (i.e., dealloying). As dealloying occurs, defects are introduced into the structure due to reaction stoichiometry: three Ag atoms are removed with deposition of one Au atom.[32] Thus, to minimize the total energy of the structure, the nanobox corners become truncated. With the addition of more $HAuCl_4$ solution, pitting is observed, resulting in Au/Ag nanocages. These porous, alloyed structures are commonly referred to as Au nanocages (Figure 1D), and the overall process is represented in Figure 1E. Please note that complete dealloying to only Au results in cage fragmentation.

In contrast, for Ag nanocubes with rounded corners (Figure 2A), Ag dissolution occurs at all cube corners (Figure 2B).[28] This difference is attributed to poly(vinyl pyrrolidone) (PVP) – the stabilizing polymer present during reaction – which interacts most strongly with {100} facets of Ag.[33] For Ag nanocubes with sharp corners, all surfaces are passivated equally with PVP; however, for Ag nanocubes with rounded corners, the {111} corners are poorly passivated in comparison to the {100} faces. These unprotected corners become primary sites for Ag dissolution, while Au deposition still occurs at the {100} faces. Thus, cubic nanocages with pores at all corners (Figure 2, C and D) are produced. This process is illustrated in Figure 2E.

Pt- and Pd-Based Nanocages

Both Na_2PtCl_4 and Na_2PdCl_4 have redox potentials (0.76 V and 0.59 V *vs.* SHE, respectively) more positive than the AgCl/Ag pair (0.22 V *vs.* SHE), indicating that Pt/Ag and Pd/Ag hollow structures can be prepared with this approach. The morphological details, however, differ from the Au system.[34] For the Pt system, nanoboxes are obtained from reaction between Ag nanocubes and Na_2PtCl_4 solution; however, the nanobox walls are composed of Pt nanoparticles, not a smooth single-crystal alloy (Figure 3A).[34] We attribute this difference to the lack of solid-solid interdiffusion between Pt and Ag at the reaction temperature.[35] Rather, when Ag nanocube pitting is initiated, Pt nanoparticles nucleate and grow on the surface without alloying, producing bumpy walls. For the Pd system, solid-solid interdiffusion is possible, resulting in Pd/Ag alloyed nanoboxes from reaction between Ag nanocubes and Na_2PdCl_4 solution (Figure 3B).[34] However, pore formation through dealloying with excess Na_2PdCl_4 is blocked, indicating that the electrochemical driving force disappears with Pd/Ag alloy formation.

Recently, we prepared porous Pd-containing nanocages by adding $HAuCl_4$ (Figure 3C).[36] In this case, Na_2PdCl_4 and $HAuCl_4$ solutions were added sequentially to the Ag nanocube suspension. The observation of pores in the final structures indicates that $HAuCl_4$ can dealloy Pd/Ag nanoboxes. Interestingly, if $HAuCl_4$ solution is administered first followed by Na_2PdCl_4, only pinholes are observed, indicating that Na_2PdCl_4 is unable to dealloy Au/Ag nanoboxes (Figure 3D). These trimetallic Pd/Au/Ag nanostructures were employed as a

catalyst for the decolorization of methyl red. Interestingly, the order in which the metal precursors were added to the Ag nanocube suspension influenced the catalytic performance of the product. In this way, galvanic replacement reactions could provide a useful means of tuning the composition of bi- and trimetallic catalysts.

Separation of Dealloying from Au Deposition

As discussed, the galvanic replacement reaction between Ag nanocubes and $HAuCl_4$ solution produces Au-containing nanocages, with much of the observed morphology attributable to reaction stoichiometry: one Au atom deposited on the template surface for every three interior Ag atoms oxidized. This relationship is also true for wall dealloying. This coupling of dealloying and Au deposition limits our control over wall thickness and nanocage porosity. It is thus desirable to de-couple these processes to achieve tighter control over these properties. By using the wet etchant $Fe(NO_3)_3$ to selectively dissolve Ag from Au/Ag alloyed nanoboxes or nanocages formed via galvanic replacement, we achieved this control.[37] Unlike dealloying with $HAuCl_4$ which involves Au deposition, the reaction between Au/Ag nanoboxes and $Fe(NO_3)_3$ is only a dealloying process:[38]

$$Ag_{(s)} + Fe(NO_3)_{3(aq)} \rightarrow AgNO_{3(aq)} + Fe(NO_3)_{2(aq)} \quad (2)$$

Figure 4A illustrates the steps of this protocol, which combines galvanic replacement and wet chemical etching. We obtain Au/Ag nanoboxes, Au/Ag nanocages, or Au cubic nanoframes, depending on the amount of etchant added to the suspension of Au/Ag nanostructures. Typically, the galvanic replacement reaction is used first to form nanoboxes (Au/Ag alloy shells with un-reacted Ag inside). Then, $Fe(NO_3)_3$ is added to dissolve remaining Ag and introduce porosity, with nanocage porosity being determined by the amount of $Fe(NO_3)_3$ added. When all the Ag is nearly removed, the central portion of each nanocage wall disappears, producing a nanoframe composed almost entirely of Au. Figure 4, B-E, shows TEM and SEM (insets) of the nanostructures obtained at each step.

Multiple-Walled Nanoshells and Nanorattles

As our approach to Au nanocages developed, it became apparent that other hollow Au-containing nanostructures could be prepared by replacing the Ag nanocubes with other Ag nanostructures. This observation has led to the synthesis of nanorings,[39] triangular nanorings,[16] prism-shaped nanoboxes,[16,40,41] and single-walled nanotubes.[40,41] Multiple-walled nanoshells and nanorattles (i.e., nanostructures consisting of shells and movable solid cores) were also demonstrated.[42] To prepare these nanostructures, a Ag layer is deposited on Au/Ag nanoshells (or solid Au/Ag particles for nanorattles) synthesized by galvanic replacement. These coated nanostructures then undergo a second galvanic replacement reaction to generate another shell. In this way, hollow Matrioshka-like structures can be prepared. The preparation of nanorattles and multiple-walled nanoshells is schematically shown in Figure 5, A and B, respectively, with corresponding TEMs in Figure 5, C and D.

Optical Properties of Au Nanocages

In addition to the compositional and morphological changes induced by the galvanic replacement reaction (or a wet etchant), the localized surface plasmon resonance (LSPR) of Au nanocages is altered and can be tuned. In Figure 6 (upper panel) are vials of Au nanocages prepared by reaction between Ag nanocubes (edge length ≈ 40 nm) and different volumes of $HAuCl_4$ solution (0.1 mM).[26,27] As the photograph and corresponding absorbance spectra (Figure 6, lower panel) indicate, the LSPR peak position of the Au nanocages is tunable

throughout the visible and into the near-infrared. This observation makes Au nanocages attractive for colorimetric sensing and biomedical applications.[43-45]

The LSPR of metal nanostructures results from incident light being scattered and absorbed at a resonant frequency due to the collective oscillation of conduction electrons.[46] The relative intensity of the scattering and absorption cross-sections of Au nanocages can be tuned by varying their size. Discrete dipole approximations (DDA) indicate that when Au nanocages are small (edge length < 45 nm), light absorption predominates; however, light scattering prevails with larger Au nanocages.[44] Thus, one must consider their size and the magnitude of their scattering and absorption cross-sections, in addition to LSPR position, when engineering nanocages for a particular application. For Au nanocages with an inner edge length of 30 nm and a wall thickness of 5 nm, the absorption cross-section is estimated as $\sim 20 \times 10^{-15}$ m^2 when tuned to 710 nm, which is much greater than traditional organic dyes (e.g., Indocyanine Green: 2.9×10^{-20} m^2 at 800 nm).[44] With such large absorption cross-sections in the near-infrared, we are engineering these nanocages for biomedical applications where the absorption of light *in vivo* could be beneficial.

Biomedical Applications of Au Nanocages

A. Targeting Cancer Cells with Au Nanocages

To be useful in biomedical applications such as cancer diagnosis and treatment, the Au nanocages must have long body circulation times and accumulate at sites of interest. Conveniently, their compact size and relative bio-inertness makes them ideal for nanomedicine applications. Additionally, their surfaces are readily modified with coatings such as poly (ethylene glycol) (PEG) or cancer-targeting moieties (e.g., antibodies or peptides) using Authiolate chemistry.[47] As an initial demonstration, Au nanocages were modified with anti-HER2 antibodies to target the epidermal growth factor receptor 2 (EGFR2 or HER2), which is over-expressed by the breast cancer cell line SK-BR-3. This bioconjugation is achieved in two-steps: *i*) Au nanocages are PEGylated by breaking the internal disulfide bond of succinimidyl propionyl poly(ethylene glycol) disulfide to form a Au-S linkage then *ii*) a PEG-antibody complex is formed through carbodiimide coupling chemistry.[48] SEM of SK-BR-3 cells incubated with antibody-modified Au nanocages confirmed their accumulation on cell surfaces. Each surface contains 460±130 Au nanocages, as determined by flow cytometry, elemental analysis, and microscopy. When incubated with unmodified Au nanocages, few Au nanocages are observed, indicating the selectivity of this approach. The bioconjugated nanocages are referred to as immuno Au nanocages.

B. Au nanocages as Contrast Enhancement Agents

The development of new and early cancer diagnostic techniques is contributing to an increase in cancer survival rates.[49] Still, for this trend to continue, new or improved methods for early detection must continue to be explored. Thus, scientists are both improving the resolution of conventional imaging techniques and developing new imaging modalities. The value of these platforms could be increased through integration with appropriate contrast enhancement agents, and our Au nanocages, with their large and tunable absorption/scattering cross-sections, represent a new class of contrast enhancement agents for optical imaging.

Optical coherence tomography (OCT) and spectroscopic optical coherence tomography (SOCT) are promising diagnostic tools for noninvasive, *in vivo* imaging, providing the micrometer resolution necessary to distinguish differences between cancerous and healthy tissues.[50,51] These systems are based on a Michelson interferometer which measures the interference signal between the backscattered light of a sample and a reference. Thus, image contrast arises primarily from the intrinsic scattering and absorption of light by tissue, but our

Au nanocages, with their large absorption/scattering cross-sections, could enhance this effect. In an initial demonstration, a tissue phantom was prepared to which Au nanocages (LSPR tuned to 716 nm) were incorporated to one half at a nM concentration.[48,52] OCT and SOCT were conducted using a 7-fs Ti:Sapphire laser with a center wavelength of 825 nm and a bandwidth of 155 nm. Imaging revealed greater light attenuation from the side containing Au nanocages. These results demonstrate the potential utility of Au nanocages as OCT contrast enhancement agents. *In vivo* studies are underway.

Recently, we demonstrated the *in vivo* use of Au nanocages as contrast enhancement agents for photoacoustic tomography (PAT).[53] PAT combines optical and ultrasonic imaging, measuring the ultrasonic waves that result from the thermoelastic expansion of tissue due to the absorption of light. It provides greater resolution than purely optical imaging in deep tissues while overcoming the disadvantages of ultrasonic imaging regarding biochemical contrast and speckle artifact.[54,55] In our initial study, PAT was used to image the cerebral cortex of a rat before and after three successive administrations of PEGylated Au nanocages. An enhancement of the brain vasculature, up to 81%, was observed (Figure 7, A and B). A difference image (Figure 7C) confirms the enhancement achieved with Au nanocage administration. A photograph of the open skull (Figure 7D) reveals that the anatomical features of the vasculature match well with those revealed by PAT. Moreover, when compared to Au nanoshells, the Au nanocages appear to be more effective contrast enhancement agents for PAT, which is likely related to their larger absorption cross-section and more compact size.[56] With their unique properties, Au nanocages should find use in other systems, such as two-photon luminescence imaging where their resistance to photobleaching is attractive.[57,58]

C. Au Nanocages for Photothermal Therapy

Au nanocages, when engineered to have large absorption cross-sections, should also display a large photothermal effect, with absorbed photons being converted into phonons (i.e., lattice vibrations) that in turn produce a localized temperature increase. We are interested in targeting this photothermal response to cancer cells as a means of cancer therapy.[59] As an initial demonstration of this photothermal effect, Au nanocages were deposited on a carbon-coated TEM grid and exposed to camera flashes. Imaging afterwards revealed that the Au nanocages had melted into spherical droplets.[60] In this case, the generated heat could not dissipate from the Au surface to the surrounding air due to poor thermal conductivity. In biological systems where thermal conductivity is greater, the generated heat should dissipate into the surroundings, rather then contribute to cage melting, thus providing a therapeutic effect when targeted to cancer cells.

We recently demonstrated *in vitro* photothermal destruction of breast cancer cells targeted with immuno Au nanocages.[61] Au nanocages 45 nm in edge length were selected because of their predicted large absorption cross-section. Their LSPR was tuned to 810 nm. SK-BR-3 cells were treated with these immuno Au nanocages then irradiated with an 810 nm laser at a power density of 1.5 W/cm^2 for 5 min. The treated cells were stained with calcein-AM and ethidium homodimer-1 so that live cells fluoresce green and dead cells fluoresce red, respectively. This analysis revealed a well-defined zone of cellular death consistent with the laser spot size (Figure 8, A and B). Cells irradiated under the same conditions but without immuno Au nanocages treatment maintained viability (Figure 8, C and D). At power densities less than 1.5 W/cm^2, the cells treated with immuno Au nanocages maintained viability. This threshold for cellular destruction is lower than that reported for Au nanoshells (35 W/cm^2) and Au nanorods (10 W/cm^2), which is likely due to the larger absorption cross-section of Au nanocages and/or their greater concentration on cell surfaces.

Concluding Remarks

The galvanic replacement reaction is a general phenomenon that can be exploited to prepare noble-metal nanocages with unique and tunable properties. We are excited about the prospected use of our Au nanocages in various biomedical applications. Owing to their relative bio-inertness, ability to be surface modified, and tunable LSPR, Au nanocages represent a new class of nanoscale agents for applications involving cancer diagnosis and treatment. Their potential use as optical contrast enhancement agents has been demonstrated, including their recent *in vivo* enhancement of PAT images. *In vitro* photothermal destruction of targeted breast cancer cells was also demonstrated with Au nanocages serving as photothermal transducers. Work is underway to expand the *in vivo* applications of the Au nanocages.

Acknowledgements

This work was supported in part by a Director's Pioneer Award (5DP1OD000798) from NIH, a fellowship from David and Lucile Packard Foundation, a DARPA-DURINT subcontract from Harvard University, and research grants from NSF and NIH. Y.X. is an Alfred P. Sloan Research Fellow (2000−2002) and a Camille Dreyfus Teacher Scholar (2002−2007). L.A. thanks the Center for Nanotechnology at UW for an IGERT Fellowship jointly sponsored by NSF and NCI. X.L. is an INEST Postdoctoral Fellow supported by Philip Morris USA (2006−2007). We thank our collaborators for their invaluable contributions to this work.

Biography

Sara E. Skrabalak received a B.S. in chemistry from Washington University in St. Louis (2002) and a Ph.D. in chemistry from the University of Illinois at Urbana-Champaign (2006), working with Professor Ken Suslick. She has been a postdoctoral researcher with Professor Younan Xia at the University of Washington since spring 2007. In fall 2008, she starts as an Assistant Professor of Chemistry at Indiana University – Bloomington. Her research interests include the synthesis/characterization of materials with novel micro- and nanostructures for environmental and biomedical applications.

Jingyi Chen received a B.S. from Sun Yat-Sen University in China (1997), a M.A. in chemistry from SUNY College at Buffalo (2002), and a Ph.D. in analytical chemistry with Professor Younan Xia from the University of Washington (2006). She is a postdoctoral fellow at Brookhaven National Laboratory.

Yugang Sun received his B.S. and Ph.D., both in chemistry, from the University of Science and Technology of China (1996 and 2001, respectively). He was a postdoctoral researcher with Professor Younan Xia at the University of Washington until 2003 and with Professor John Rogers at the University of Illinois at Urbana-Champaign until 2006. He is a staff scientist at Argonne National Laboratory. His research interests include synthesis/characterization of nanostructures, micro/nanofabrication, bioanalysis, and devices for photonics and electronics.

Xianmao Lu received B.S. and M.S. degrees in Chemical Engineering from Tsinghua University, China. He received his Ph.D. in Chemical Engineering from the University of Texas at Austin (2005) working with Professors Keith Johnston and Brian Korgel. He is a postdoctoral researcher with Professor Younan Xia at Washington University in St. Louis. His research interests include synthesis/processing of metal and semiconductor nanostructures.

Leslie Au received B.S. degrees in chemistry and biology (2005) and a M.A. in chemistry (2007) from the University of Washington. She is pursuing her Ph.D. in chemistry at the University of Washington with Professor Younan Xia. Her research interests include the synthesis/use of metal nanostructures for biomedical research.

Claire M. Cobley graduated with a B.S. in chemistry from Brown University (2006) and a M.S. in chemistry from the University of Washington (2007). She is pursuing her Ph.D. in Biomedical Engineering with Younan Xia at Washington University in St. Louis. Her research interests include the synthesis, analysis, and applications of metal nanostructures.

Younan Xia was born in Jiangsu, China, in 1965. He received a B.S. in chemical physics from the University of Science and Technology of China in 1987 then worked as a graduate student for four years at the Fujian Institute of Research on the Structure of Matter, Chinese Academy of Sciences. He came to the United States in 1991, received a M.S. in inorganic chemistry from the University of Pennsylvania (with the late Professor Alan G. MacDiarmid) in 1993, and a Ph.D. in physical chemistry from Harvard University (with Professor George M. Whitesides) in 1996. After a short stint as a postdoctoral fellow with Professors George M. Whitesides and Mara Prentiss, he started as an Assistant Professor of Chemistry at the University of Washington. He was promoted to Associated Professor and Professor in 2002 and 2004, respectively. He moved to Washington University in St. Louis in fall 2007 and is now the James M. McKelvey Professor of Biomedical Engineering. His research interests include nanostructured materials, nanomedicine, biomaterials, self-assembly, photonic crystals, colloidal science, surface modification, and electrospinning.

References

1. Shipway AN, Katz E, Willner I. Nanoparticle arrays on surfaces for electronic, optical, and sensor applications. ChemPhysChem 2000;1:18–52.
2. Murphy CJ, San TK, Gole AM, Orendorff CJ, Gao JX, Gou L, Hunyadi SE, Li T. Anisotropic metal nanoparticles: synthesis, assembly, and optical applications. J. Phys. Chem. B 2005;109:13857–13870. [PubMed: 16852739]
3. Willets KA, Van Duyne RP. Localized surface plasmon resonance spectroscopy and sensing. Annu. Rev. Phys. Chem 2007;58:267–297. [PubMed: 17067281]
4. Aiken JD, Finke RG. A review of modern transition-metal nanoclusters: their synthesis, characterization, and applications in catalysis. J. Mol. Catal. A-Chem 1999;145:1–44.
5. Murray CB, Kagan CR, Bawendi MG. Synthesis and characterization of monodisperse nanocrystals and close-packed nanocrystal assemblies. Annu. Rev. Mater. Sci 2000;30:545–610.
6. Wiley B, Sun Y, Xia Y. Synthesis of silver nanostructures with controlled shapes and properties. Acc. Chem. Res 2007;40:1067–1076. [PubMed: 17616165]
7. Noguez C. Surface plasmons on metal nanoparticles: the influence of shape and physical environment. J. Phys. Chem. C 2007;111:3806–3819.
8. Hu M, Chen J, Li Z-Y, Au L, Hartland GV, Li X, Marquez M, Xia Y. Gold nanostructures: engineering their plasmonic properties for biomedical applications. Chem. Soc. Rev 2006;35:1084–1094. [PubMed: 17057837]
9. El-Sayed MA. Some interesting properties of metals confined in time and nanometer space of different shapes. Acc. Chem. Res 2001;34:257–264. [PubMed: 11308299]
10. Xia Y, Yang P, Sun Y, Wu Y, Mayers B, Gates B, Yin Y, Kim F, Yan H. One-dimensional nanostructures: synthesis, characterization, and applications. Adv. Mater 2003;15:353–389.
11. Jana NR, Gearheart L, Murphy CJ. Wet chemical synthesis of silver nanorods and nanowires of controllable aspect ratio. Chem. Commun 2001:617–618.
12. Jana NR, Gearheart L, Murphy CJ. Wet chemical synthesis of high aspect ratio cylindrical gold nanorods. J. Phys. Chem. B 2001:4065–4067.
13. Kim F, Song JH, Yang P. Photochemical synthesis of gold nanorods. J. Am. Chem. Soc 2002;124:14316–14317. [PubMed: 12452700]
14. Jackson JB, Halas NJ. Silver nanoshells: variations in morphologies and optical properties. J. Phys. Chem. B 2001;105:2743–2746.
15. Chen SH, Carrol DL. Synthesis and characterization of truncated triangular silver nanoplates. Nano Lett 2002;2:1003–1007.

16. Sun Y, Xia Y. Triangular nanoplates of silver: synthesis, characterization, and use as sacrificial templates for generating triangular nanorings of gold. Adv. Mater 2003;15:695–699.
17. Shao Y, Jin Y, Dong S. Synthesis of gold nanoplates by aspartate reduction of gold chloride. Chem. Commun 2004:1004–1105.
18. Sun Y, Xia Y. Shape-controlled synthesis of gold and silver nanoparticles. Science 2002;298:2176–2179. [PubMed: 12481134]
19. Xiong Y, Chen J, Wiley B, Xia Y, Yin Y, Li Z-Y. Size-dependence of surface plasmon resonance and oxidation for Pd nanocubes synthesized via a seed etching process. Nano Lett 2005;5:1237–1242. [PubMed: 16178217]
20. Huang C, Wang Y, Chiu P, Shih M, Meen T. Electrochemical synthesis of gold nanocubes. Mater. Lett 2006;60:1896–1900.
21. Wiley B, Xiong Y, Li Z-Y, Yin Y, Xia Y. Right bipyramids of silver: a new shape derived from single twinned seeds. Nano Lett 2006;6:765–768. [PubMed: 16608280]
22. Wiley BJ, Chen Y, McLellan JM, Xiong Y, Li Z-Y, Ginger D, Xia Y. Synthesis and optical properties of silver nanobars and nanorice. Nano Lett 2007;7:1032–1036. [PubMed: 17343425]
23. Zettsu N, McLellan JM, Wiley B, Yin Y, Li Z-Y, Xia Y. Synthesis, stability, and surface plasmonic properties of rhodium multipods, and their use as substrates for surface-enhanced Raman scattering. Angew. Chem. In. Edit 2006;45:1288–1292.
24. Lu X, Chen J, Skrabalak SE, Xia Y. Galvanic replacement reaction: a simple and powerful route to hollow and porous metal nanostructures. P. I. Mech. Eng. N – J. Nanoeng. Nanosys 2007;221in press
25. With the high Cl^- concentration during galvanic replacement, we suggest that at the reaction site AgCl nano-crystallites form then dissolve into the solvent at reaction temperature. The reduction potentials reported are referenced to the SHE; however, galvanic replacement reactions are run at elevated temperatures under unique conditions. Thus, the absolute electrochemical potential difference in our systems could deviate from anticipated, but we include quantitative values to better illustrate the principles that underlie this work
26. Skrabalak SE, Au L, Li X, Xia Y. Facile synthesis of Ag nanocubes and Au nanocages. Nature Prot 2007;2:2182–2190.
27. Sun Y, Xia Y. Mechanistic study on the replacement reaction between silver nanostructures and chloroauric acid in aqueous medium. J. Amer. Chem. Soc 2004;126:3892–3901. [PubMed: 15038743]
28. Chen J, McLellan JM, Siekkinen A, Xiong Y, Li Z-Y, Xia Y. Facile synthesis of gold-silver nanocages with controllable pores on the surface. J. Amer. Chem. Soc 2006;128:14776–14777. [PubMed: 17105266]
29. Wang Z-L. Transmission electron microscopy of shape-controlled nanocrystals and their assemblies. J. Phys. Chem. B 2000;104:1153–1175.
30. Shibata T, Bunker BA, Zhang Z, Meisel D, Vardeman CF, Gezelter JD. Size-dependent spontaneous alloying of Au-Ag nanoparticles. J. Amer. Chem. Soc 2002;124:11989–11996. [PubMed: 12358545]
31. Wonnell SK, Delaye JM, Bibole M, Limoge Y. Activation volume for the interdiffusion of Ag-Au multilayers. J. Appl. Phys 1992;72:5195–5205.
32. Erlenbacher J, Aziz MJ, Karma A, Dimitrov N, Sieradzki K. Evolution of nanoporosity in dealloying. Nature 2001;410:450–453. [PubMed: 11260708]
33. Sun Y, Mayers B, Herricks T, Xia Y. Polyol synthesis of uniform silver nanowires: A plausible growth mechanism and the supporting evidence. Nano Lett 2003;3:955–960.
34. Chen J, Wiley B, McLellan JM, Xiong Y, Li Z-Y, Xia Y. Optical properties of Pd-Ag and Pt-Ag nanoboxes synthesized via galvanic replacement reactions. Nano Lett 2005;5:2058–2062. [PubMed: 16218737]
35. Batzill M, Koel BE. Silver of Pt(100) – room temperature growth and high temperature alloying. Surf. Sci 2004;553:50–60.
36. Cobley CM, Campbell DJ, Xia Y. Tailoring the optical and catalytic properties of gold-silver nanoboxes and nanocages by introducing palladium. Adv. Mater. 2007in press
37. Lu X, Au L, McLellan J, Li Z-Y, Marquez M, Xia Y. Fabrication of cubic nanocages and nanoframes by dealloying Au/Ag alloy nanoboxes with an aqueous etchant based on $Fe(NO_3)_3$ or NH_4OH. Nano Lett 2007;7:1764–1769. [PubMed: 17489641]

38. Xia Y, Kim E, Whitesides GM. Microcontact printing of alkanethiols on silver and its application in microfabrication. J. Electrochem. Soc 1996;143:1070–1079.
39. Lu X, Tuan H-Y, Chen J, Li Z-Y, Korgel BA, Xia Y. Mechanistic studies on the galvanic replacement reaction between multiply twinned particles of Ag and $HAuCl_4$ in an organic medium. J. Am. Chem. Soc 2007;129:1733–1742. [PubMed: 17243691]
40. Sun Y, Mayers B, Xia Y. Template-engaged replacement reaction: a one-step approach to the large-scale synthesis of metal nanostructures with hollow interiors. Nano Lett 2002;2:481–485.
41. Sun Y, Mayers B, Xia Y. Metal nanostructures with hollow interiors. Adv. Mater 2003;15:641–646.
42. Sun Y, Wiley BJ, Li Z-Y, Xia Y. Synthesis and optical properties of nanorattles and multiple-walled nanoshells/nanotubes made of metal alloys. J. Am. Chem. Soc 2004;126:9399–9406. [PubMed: 15281832]
43. Elghanian R, Storhoff JJ, Mucic RC; Letsinger RL, Mirkin CA. Selective colorimetric detection of polynucleotides based on the distance-dependent optical properties of gold nanoparticles. Science 1997;227:1078–1081. [PubMed: 9262471]
44. Skrabalak SE; Chen J, Au L, Lu X, Li X, Xia Y. Gold nanocages for biomedical applications. Adv. Mater 2007;19:3177–3184.
45. Skrabalak SE, Au L, Lu X, Li X, Xia Y. Gold nanocages for cancer detection and treatment. Nanomed 2007;2:657–668. [PubMed: 17976028]
46. Kreibig, U.; Vollmer, M. Optical Properties of Metal Clusters. Springer; Berlin: 1995.
47. Xia Y, Rogers JA, Paul KE, Whitesides GM. Unconventional methods for fabricating and patterning nanostructures. Chem. Rev 1999;99:1823–1848. [PubMed: 11849012]
48. Chen J, Saeki F, Wiley B, Cang H, Cobb MJ, Li Z-Y, Au L, Zhang H, Kimmey MB, Li X, Xia Y. Gold nanocages: bioconjugation and their potential use as optical imaging contrast agents. Nano Lett 2005;5:473–477. [PubMed: 15755097]
49. Jemal A, Murray T, Ward E, Samuels A, Tiwari RC, Ghafoor A, Feuer EJ, Thun MJ. Cancer statistics 2005. Cancer J. Clin 2005;55:10–30.
50. Huang D, Swanson EA, Lin CP; Schuman JS, Stinson WG, Chang W, Hee MR, Flotte T, Gregory K, Puliafito CA. Optical coherence tomography. Science 1991;254:1178–1181. [PubMed: 1957169]
51. Fujimoto JG. Optical coherence tomography for ultrahigh resolution *in vivo* imaging. Nat. Biotechnol 2003;21:1361–1367. [PubMed: 14595364]
52. Cang H, Sun T, Chen J, Wiley BJ, Xia Y, Li X. Gold nanocages as potential contrast agents for spectroscopic and conventional optical coherence tomography. Opt. Lett 2005;30:3048–3050. [PubMed: 16315717]
53. Yang X, Skrabalak SE, Li Z-Y, Xia Y, Wang LV. Photoacoustic tomography of a rat cerebral cortex *in vivo* with Au nanocages as an optical contrast agent. Nano Lett 2007;7:3798–3802. [PubMed: 18020475]
54. Ku G, Wang LV. Deeply penetrating photoacoustic tomography in biological tissues enhanced with an optical contrast agent. Opt. Lett 2005;30:507–509. [PubMed: 15789718]
55. Ku G, Fornage BD, Jin X, Xu M, Hunt KK, Wang LV. Thermoacoustic and photoacoustic tomography of thick biological tissues toward breast imaging. Technol. Cancer Res. Treat 2005;4:559–566. [PubMed: 16173826]
56. Wang Y, Xie X, Wang X, Ku G, Gill KL, O'Neal DP, Stocia G, Wang LV. Photoacoustic tomography of a nanoshell contrast agent in the *in vivo* rat brain. Nano Lett 2004;4:1689–1692.
57. Wang H, Huff TB, Zweifel DA, He W, Low PS, Wei A, Cheng J-X. *In vitro* and *in vivo* two-photon luminescence imaging of single gold nanorods. Proc. Natl. Acad. Sci. USA 2005;102:15752–15756. [PubMed: 16239346]
58. Durr NJ, Larson T, Smith DK, Korgel BA, Sokolov K, Ben-Yakar A. Two-photon luminescence imaging of cancer cells using molecularly targeted gold nanorods. Nano Lett 2007;7:941–945. [PubMed: 17335272]
59. Anderson RR, Parrish JA. Selective photothermolysis – precise microsurgery by selective absorption of pulsed radiation. Science 1983;220:524–527. [PubMed: 6836297]
60. Chen J, Wiley B, Li Z-Y, Cang H, Campbell D, Saeki F, Au L, Lee J, Li X, Xia Y. Gold nanocages: engineering their structure for biomedical applications. Adv. Mater 2005;17:2255–2261.

61. Chen J, Wang D, Xi J, Au L, Siekkinen A, Warsen A, Li Z-Y, Zhang H, Xia Y, Li X. Immuno gold nanocages with tailored optical properties for targeted photothermal destruction of cancer cells. Nano Lett 2007;7:1318–1322. [PubMed: 17430005]

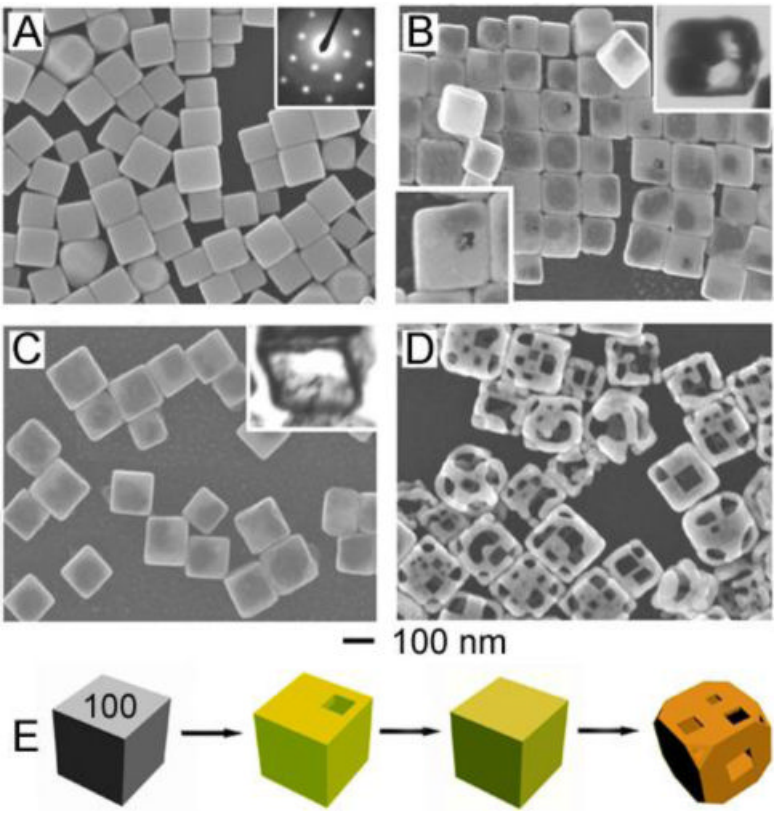

FIGURE 1.

(A) SEM of Ag nanocubes. Inset: electron diffraction indicates they are single-crystals. (B) SEM of product after 0.30 mL of 1 mM $HAuCl_4$ solution was added to a 5-mL 0.8 mM Ag nanocube suspension; a pinhole (lower inset) is observed on the exposed face of ~1 in 6 nanocubes. Upper inset: TEM of a microtomed sample reveals early hollowing out. (C) SEM of product after 0.50 mL of $HAuCl_4$ solution was added. Inset: TEM of a microtomed sample reveals the hollow interior of the nanobox. (D) SEM of product after 2.25 mL of $HAuCl_4$ solution was added. Porous nanocages produced. (E) Illustration summarizing morphological changes. Coloration indicates the conversion of a Ag nanocube into a Au/Ag nanobox then a predominately Au nanocage.[27]

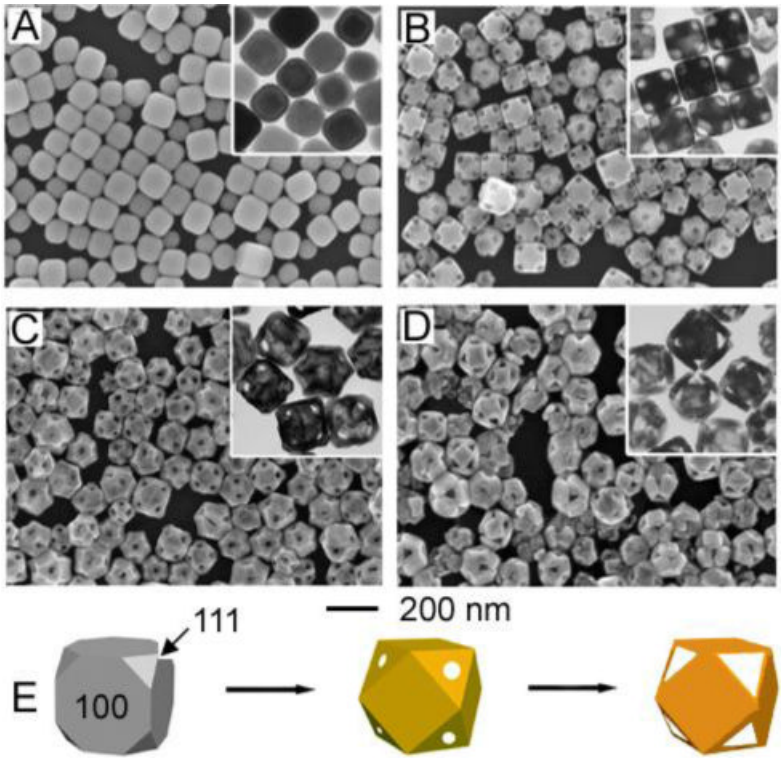

FIGURE 2.

SEM and TEM (inset) (A) of Ag nanocubes with rounded corners and (B-D) product after reaction with 0.6, 1.6, and 3.0 mL of 0.1 mM $HAuCl_4$ solution, respectively. (E) Illustration summarizing morphological changes. Coloration indicates conversion of a Ag nanocube into a Au/Ag nanocage then a predominately Au nanocage.[28]

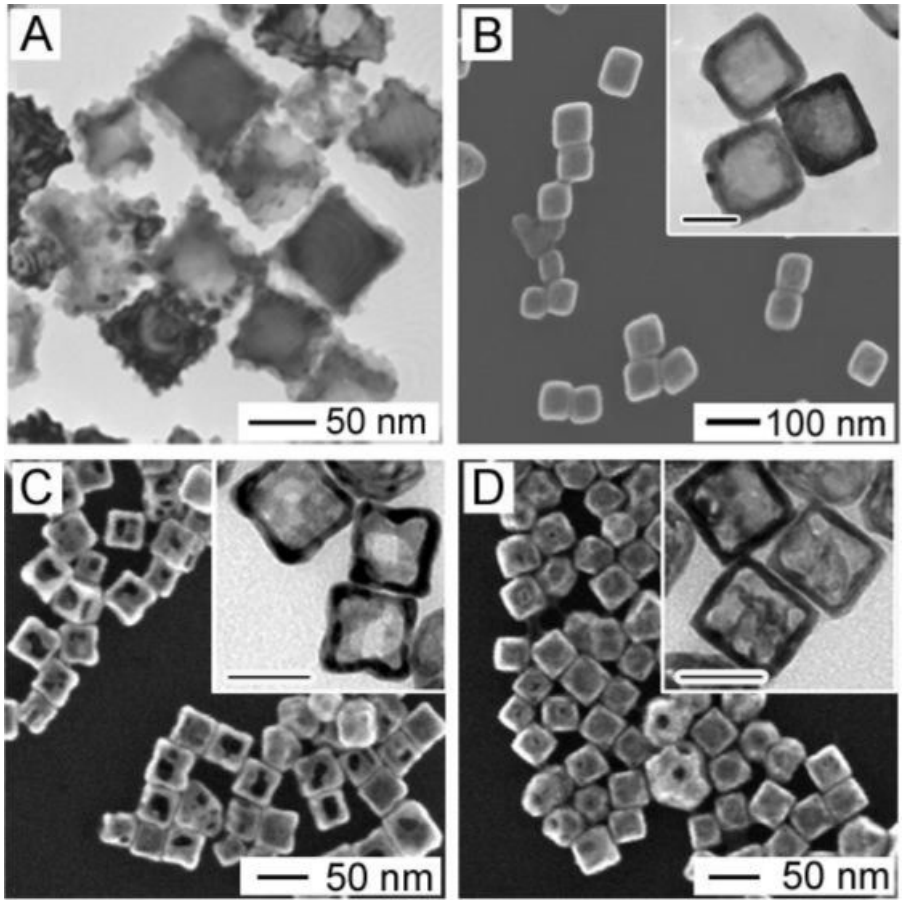

FIGURE 3.

(A) TEM of Pt/Ag nanoboxes from the galvanic replacement reaction between Ag nanocubes and Na_2PtCl_4 solution. (B) SEM and TEM (inset) of Pd/Ag nanoboxes from the galvanic replacement reaction between Ag nanocubes and Na_2PdCl_4 solution. (C) and (D) SEM and TEM (inset) of Ag/Au/Pd nanocages from the galvanic replacement reaction between Ag nanocubes and (C) Na_2PdCl_4 solution, followed by $HAuCl_4$ solution and (D) $HAuCl_4$ solution, followed by Na_2PdCl_4 solution. Inset scale bars = 40 nm.[34,36]

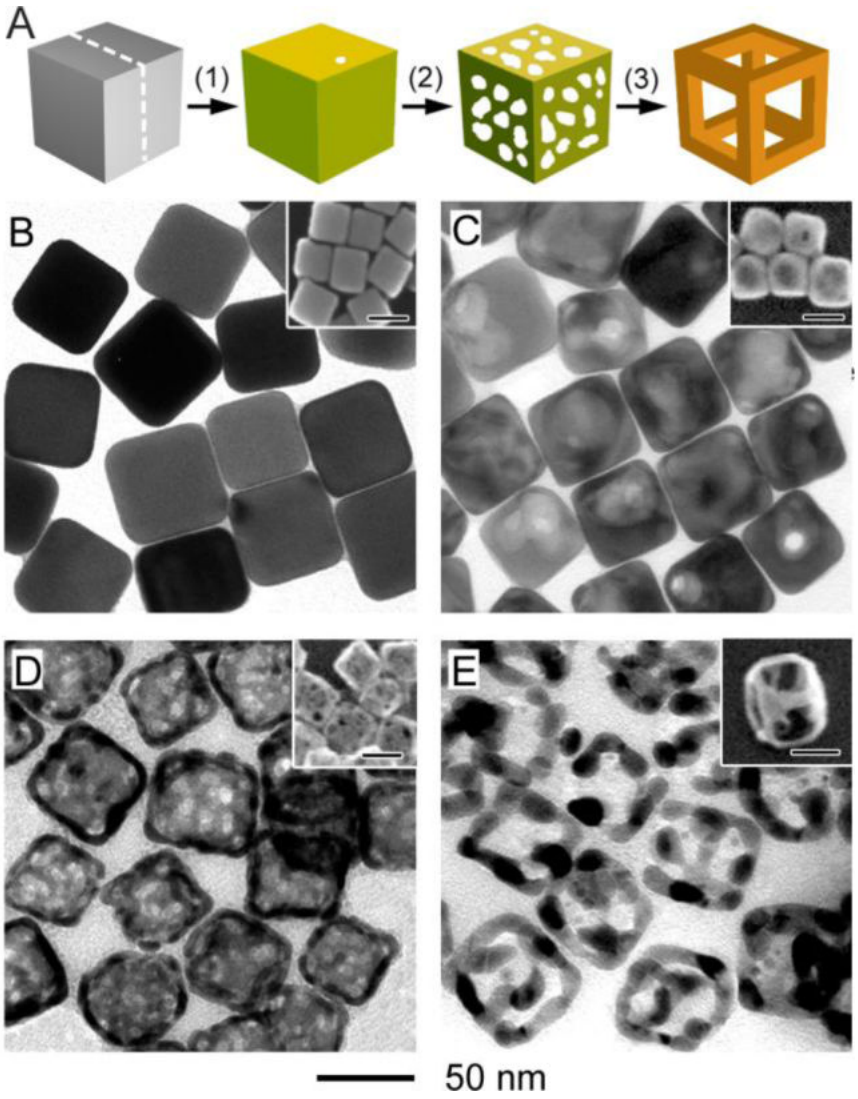

FIGURE 4.

(A) Illustration summarizing cubic Au nanoframe formation. Beginning with Ag nanocubes, Au/Ag nanoboxes are prepared by galvanic replacement (step 1). Then a wet etchant removes remaining Ag to form a porous nanocage (step 2), which with more etchant, evolves into a cubic nanoframe (step 3). (B-E) TEM and SEM (inset) of (B) 50 nm Ag nanocubes, (C) Au/Ag nanoboxes prepared by galvanic replacement, and (D) nanocages and (E) nanoframes prepared with $Fe(NO_3)_3$ as a Ag etchant. Coloration indicates the conversion of a Ag nanocube into a Au/Ag nanocage then a predominately Au nanocage.[37]

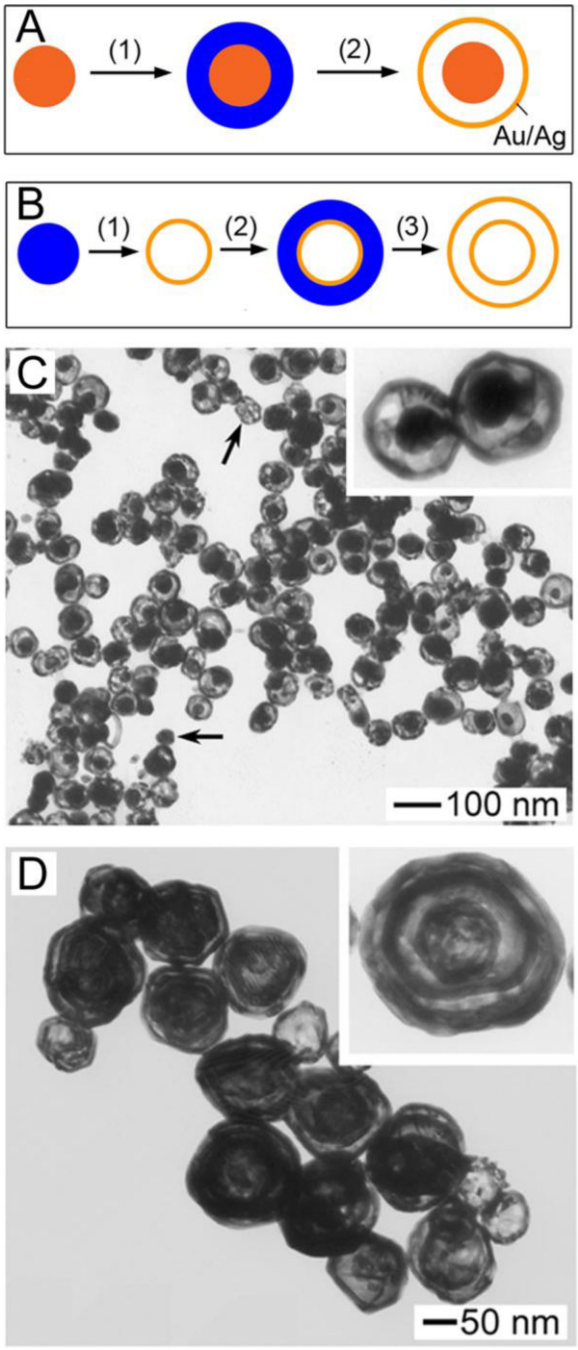

Figure 5.
(A) Schematic illustrating the multi-step preparation of nanorattles. To a Au/Ag (in orange) nanoparticle, Ag (in blue) is deposited on its surface; the galvanic replacement reaction with $HAuCl_4$ then transforms the Ag layer into a Au/Ag shell. (B) Schematic illustrating the multi-step preparation of multiple-walled nanoshells, beginning with a Ag nanoparticle. (C) TEM of nanorattles. (D) TEM of multiple-walled Au/Ag nanoshells.[42]

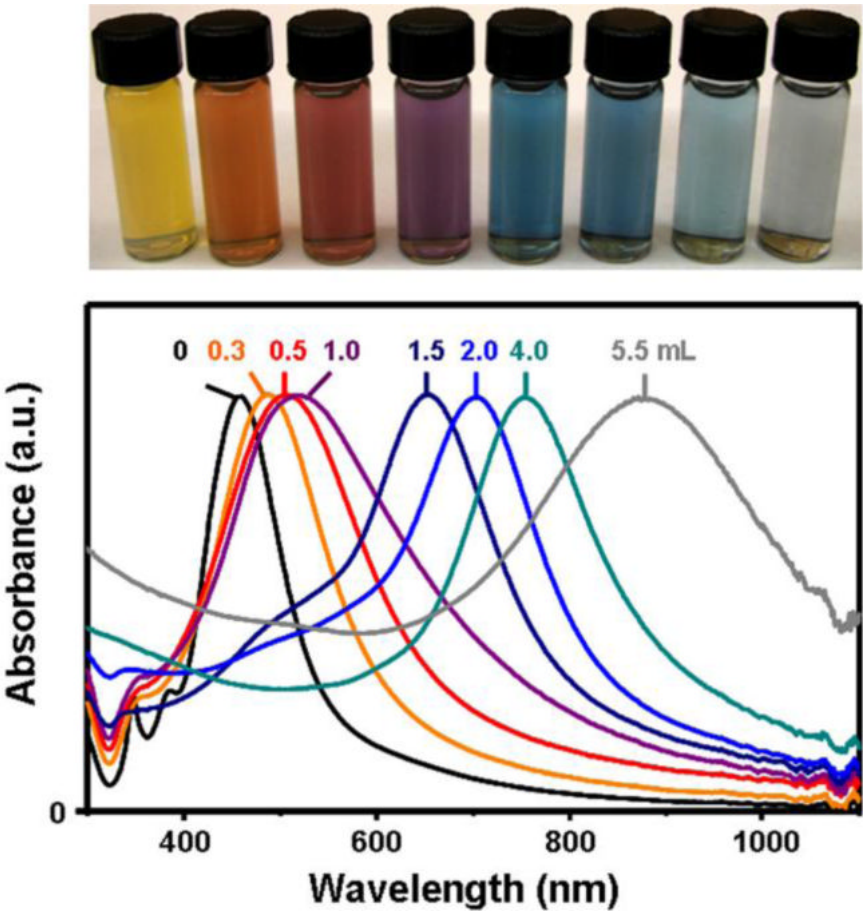

FIGURE 6.

Top panel: vials containing Au nanocages prepared by reacting 5 mL of a ~0.2 nM Ag nanocube (edge length: 40 nm) suspension with different volumes of a 0.1 mM $HAuCl_4$ solution. Lower panel: the corresponding UV-visible absorbance spectra of Ag nanocubes and Au nanocages.

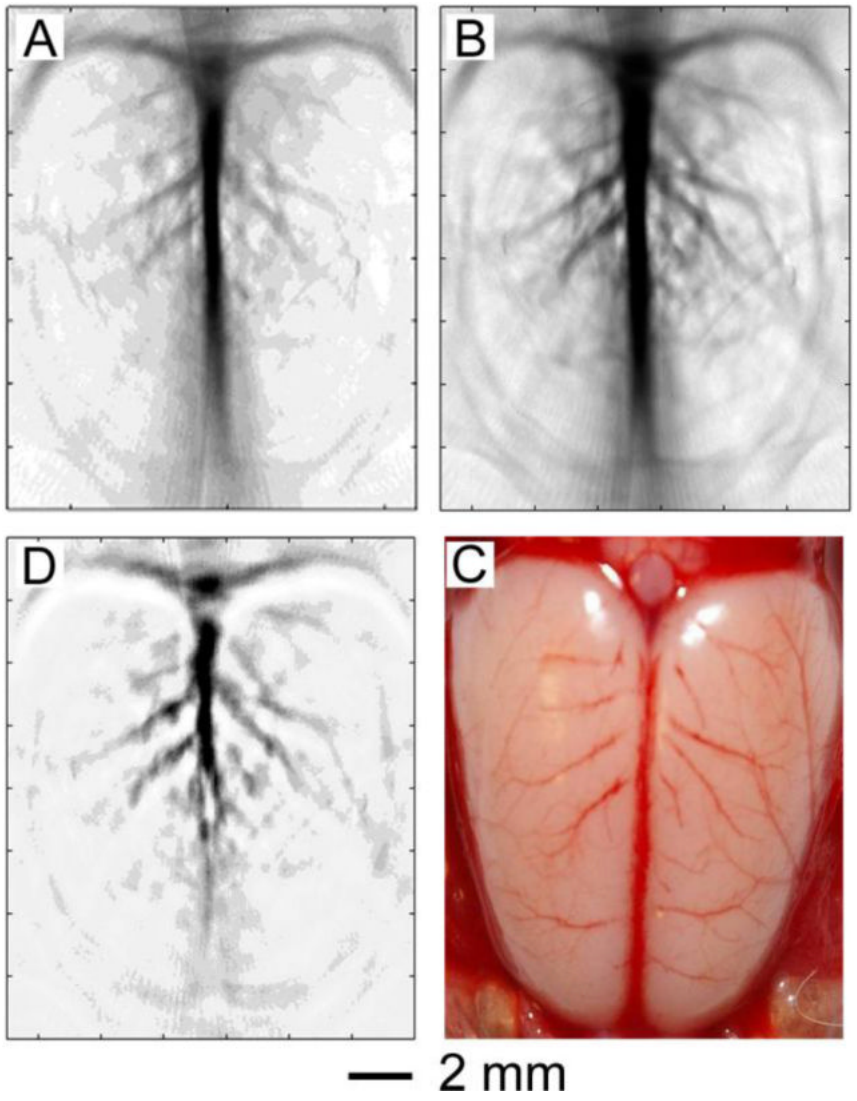

FIGURE 7.

PAT of a rat's cerebral cortex (A) before and (B) ~2 h after the final injection of PEGylated Au nanocages (the peak enhancement point). (C) A differential PAT image. (D) A open-skull photograph of the rat's cerebral cortex, revealing features of the vasculature.[53]

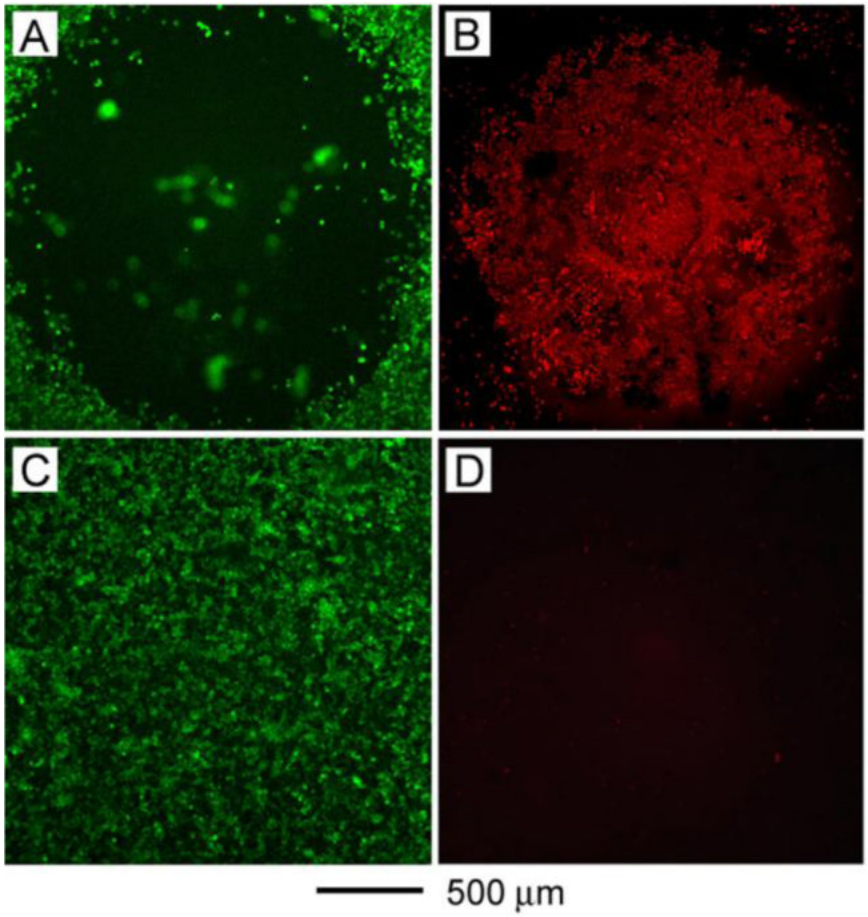

FIGURE 8.

(A) and (B) SK-BR-3 breast cancer cells treated with immuno Au nanocages then irradiated with 810 nm light at a power density of 1.5 W/cm^2 for 5 min. A well-defined zone of cellular death revealed by (A) calcein AM (green fluorescence indicates live cells) and (B) ethidium homodimer-1 (EthD-1, red fluorescence indicates dead cells) assays. (C) and (D) SKBR-3 cells irradiated under the same conditions but without immuno Au nanocages treatment. The cells maintained viability, indicated by (C) calcein AM and (D) EthD-1 assays.[61]